

Article

# Evaluation Method for Energy Saving of Sail-Assisted Ship Based on Wind Resource Analysis of Typical Route

Ranqi Ma, Zhongyi Wang, Kai Wang \*, Haoyang Zhao, Baoshen Jiang, Yize Liu, Hui Xing  and Lianzhong Huang \*

Marine Engineering College, Dalian Maritime University, Dalian 116026, China;  
maranqi1989@dltmu.edu.cn (R.M.); dlmuwzy@dltmu.edu.cn (Z.W.); abc998866@dltmu.edu.cn (H.Z.);  
1120211160jbs@dltmu.edu.cn (B.J.); lyz\_dmu@dltmu.edu.cn (Y.L.); xingcage@dltmu.edu.cn (H.X.)

\* Correspondence: kwang@dltmu.edu.cn (K.W.); huanglz@dltmu.edu.cn (L.H.)

**Abstract:** Sail-assisted technology can reduce greenhouse-gas emissions by saving the energy consumption of ships with wind energy utilization. The distribution characteristics of marine wind resources are critical to the energy-saving effect of sail-assisted ships. However, due to the lack of effective energy-saving evaluation methods for improving the utilization rate of wind energy, a high potential for wind energy utilization still exists. A novel energy-saving evaluation method based on the wind energy resource analysis of typical ship routes is proposed in this paper. First, a three-degree-of-freedom motion model for sail-assisted ships considering the wing sail forces is constructed. Then, a wind resource acquisition and analysis method based on spatial-temporal interpolation is proposed. On this basis, the wind field probability matrix and wing sail force matrix are established. Ultimately, an energy-saving evaluation method for sail-assisted ships on typical routes is proposed by combining the sailing condition of ships. The case study results show that the energy-saving effect of a wing sail-assisted oil tanker that sailed on the China-to-Middle East route was more than 5.37% in 2021 and could reach 9.54% in a single voyage. It is of great significance to realize the popularization and application of sail-assisted technology, thus improving the greenization of the shipping industry.



**Citation:** Ma, R.; Wang, Z.; Wang, K.; Zhao, H.; Jiang, B.; Liu, Y.; Xing, H.; Huang, L. Evaluation Method for Energy Saving of Sail-Assisted Ship Based on Wind Resource Analysis of Typical Route. *J. Mar. Sci. Eng.* **2023**, *11*, 789. <https://doi.org/10.3390/jmse11040789>

Academic Editor: Alessandro Ridolfi

Received: 4 March 2023

Revised: 31 March 2023

Accepted: 3 April 2023

Published: 5 April 2023



**Copyright:** © 2023 by the authors. Licensee MDPI, Basel, Switzerland. This article is an open access article distributed under the terms and conditions of the Creative Commons Attribution (CC BY) license (<https://creativecommons.org/licenses/by/4.0/>).

## 1. Introduction

As one of the most important ways of transportation, most of the global trade volume is carried out by shipping [1]. With the increase in global shipping trades, the consumption of marine fossil fuels also significantly increases, leading to more air pollution and greenhouse gases [2,3]. The carbon emissions from shipping are also increasing annually [4,5]. The International Maritime Organization (IMO) pointed out that the greenhouse-gas emissions of the shipping industry were 1.076 billion tons in 2018, and the proportion of the shipping industry in global emissions increased from 2.76% in 2012 to 2.89% in 2018. With the increasing demand for maritime transportation, the emissions of carbon dioxide are expected to increase by about 50% in 2050 compared with 2018 [6]. Therefore, energy conservation and emission reduction measures should be taken in time; otherwise, the carbon emissions of the shipping industry will sharply rise in the future. In response to climate change and carbon emission growth, various organizations and companies have put forward emission reduction targets [7]. The IMO has introduced the existing ship energy efficiency index (EEXI) and the carbon emission intensity index (CII) after the ship energy efficiency operation index (EEOI) and the ship energy efficiency management plan (SEEMP) to reduce shipping carbon emissions [8].

The shipping industry has put forward a variety of countermeasures to reduce the carbon dioxide emissions from ships [9,10], including clean energy [11–13], alternative

fuels [14,15], collaborative optimization of ship energy efficiency [16–18], hull optimization, and power system optimization [19]. As a kind of clean energy, wind energy can significantly improve the energy-saving effect and reduce emissions [9,20]. Wind energy is widely distributed around the world, and there are wind resources at almost any time and anywhere in the ocean [21,22]. Moreover, regarding wind energy, as a kind of renewable energy, it has become a trend for ships to use wind energy to realize emission reduction [23]. Due to its advantages in environmental protection and energy-saving effect, the Wind-Assisted Propulsion System (WAPS) has become a hotspot in the shipping industry [24]. Wing sails use wind energy to generate thrust force as auxiliary thrust for the ship, thus reducing fuel consumption and achieving the emission reduction purpose.

The effect of emission reduction should take the sailing condition of the ship, the aerodynamic characteristics of the sail, and the navigation meteorological characteristics into account. On the same route, due to the uncertainty of the marine wind field, the wind field where a sail-assisted ship sails may have different spatial and temporal distribution characteristics. The auxiliary thrust force of wing sails varies with different relative wind directions and speeds according to the aerodynamic characteristic of the sails. Therefore, the effect of energy saving is comprehensively influenced by ship condition, sailing route, sailing speed, types of sails, sailing time, sailing sea area, and wind resources. It is essential to evaluate the wing sail thrust effect on the ship route to realize the maximum emission reduction effect of ships, as well as improve the green level of ships.

It is necessary to combine the ship route information, environment, and ship hydrodynamic model to study the energy efficiency improvement effect of ships. Morvan et al. [25] constructed a hydrodynamic simulation model of a sailing boat and discussed the calculation method of the lateral force of the sail and rudder resistance. Du et al. [26] used improved 3D dynamic programming (3DDP) to optimize the route of ocean-going ships according to weather conditions and technical specifications. They planned an optimal solution of route-speed planning according to weather conditions, speed, main-engine power, and other constraints. Kramer et al. [27] studied a wing sail-assisted cargo ship on a Nordic coastal route, analyzed the variation law of hydrodynamic force with ship speed, rudder angle, heading angle, and propeller load using computational fluid dynamics (CFD). They analyzed the wave resistance of the propeller using the empirical method and studied the fuel saving of wind-assisted navigation by combining the route simulation framework with weather data. The aerodynamic characteristics as well as thrust performance of a multi-wing sail with different attack angles, flap lengths, and deflection angles were studied by Lee et al. [28] with CFD. Li et al. [29] measured the lift and resistance of the ship wing sails at different inclination angles and different angles of attack with a wind generator. They studied the aerodynamic interaction among multiple sails and analyzed the sailing performance of the ship, such as rudder angle and heading angle, under wind influence. Elger et al. [30] studied the calculation of lateral force caused by the sailing drift angle and rudder angle during sailing. They put forward a calculation method for the lateral force of a sailing boat and verified its effectiveness with the towing model test. Sauder et al. [31] established the performance index of sail-assisted navigation when a ship sails under a stable wind profile with different directions and speeds. They analyzed the propeller working efficiency and studied the wing sail thrust effect at different wind angles. Ma et al. [32] calculated the wing sail performance using multi-point theory, the CFD test, and the EEDI by coupling the optimization of the sail aerodynamic performance, which proved the effectiveness of sail-assisted technology in improving ship energy efficiency.

Current studies mostly focus on sail aerodynamic performance optimization, ship route, and speed optimization, and there is still a lack of effective energy-saving evaluation methods for sail-assisted ships based on the distribution characteristics of wind resources on ship routes. This paper made two contributions in the following aspects:

- (1) A wind resource acquisition method based on the longitude, latitude, and time of the route is proposed to convert the regional marine wind resources into wind resources on sailing routes according to marine wind field data. The level of available wind

resources on a specific route of a sail-assisted ship is determined by combining wind resource analysis and the navigation condition, as well as the wing sail force.

- (2) An energy-saving evaluation method considering wind resource distribution on the route, the navigation condition of the ship, wing sail aerodynamic characteristics, and wing sail thrust characteristics is proposed. The energy-saving evaluation of sail-assisted ships on a typical route is realized by establishing the wing sail thrust force matrix, which contributes to promote the green development and decarbonization of the shipping industry.

In the following, Section 2 introduces the energy-saving evaluation methods for sail-assisted ships, including a mathematical model, the force analysis of wing sails, the analysis method of wind resources, and the wing sail force matrix on the ship route. The verification of the motion model of a sail-assisted very large crude carrier (VLCC), the wind resource spatial-temporal distribution characteristic analysis of the VLCC in the sailing area, and the discussion on the energy-saving effect under different sailing conditions are presented in Section 3 with a case study. Finally, Section 4 gives the conclusions and future work.

## 2. Methodology

### 2.1. Force Analysis and Mathematical Model of Wing Sail-Assisted Ship

In wing sail-assisted ships, the propeller converts main-engine output power into thrust force to propel the ship, and the wing sails also contribute part of the auxiliary propulsion to reduce the output power, thus achieving the purpose of fuel consumption saving. Meanwhile, the ship needs to overcome wind resistance and the resistance composed of static water resistance, additional resistance, added resistance of waves, etc., to achieve normal navigation, as shown in Figure 1.

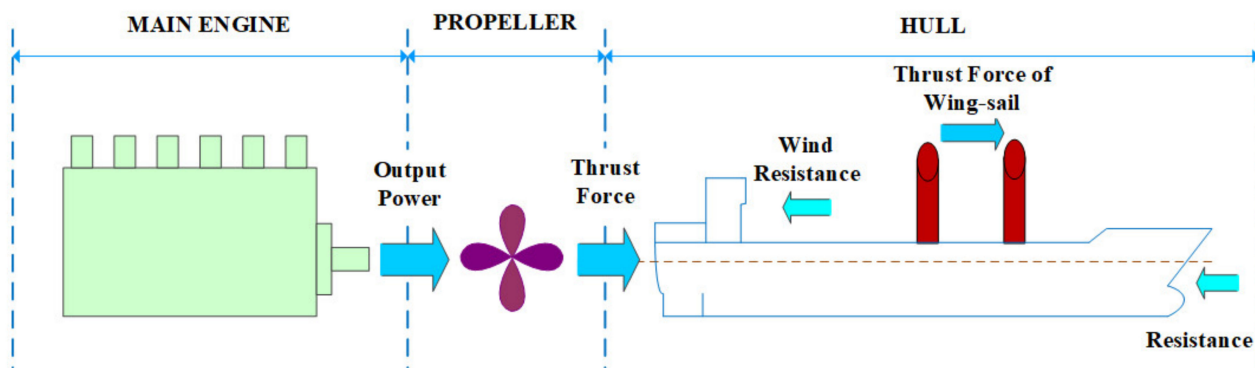


**Figure 1.** Force analysis diagram of wing sail-assisted ship.

According to the separate model proposed by the Japanese Marine Modeling Group (MMG) [33], a three-degree-of-freedom model of a wing sail-assisted ship was constructed to calculate the force and power of wing sail-assisted ships.

The ship motion is described both in the right-hand-side Cartesian Earth coordinate system and the ship-following coordinate system, as shown in Figure 2, where G stands for center of gravity. The differential equations of kinematics and dynamics are obtained by combining the influence of the sail, as shown in Equations (1) and (2).

$$\begin{cases} \dot{x}_0 = u \cos \psi - v \sin \psi \\ \dot{y}_0 = u \sin \psi + v \cos \psi \\ \dot{\psi} = r \end{cases} \quad (1)$$

$$\begin{cases} (m + m_x)\dot{u} - (m + m_y)v = X_H + X_P + X_R + X_W + X_S \\ (m + m_y)\dot{v} + (m + m_x)u = Y_H + Y_R + Y_W + Y_S \\ (I_{zz} + J_{zz})\dot{r} = N_H + N_R + N_W + N_S \\ 2\pi(I_{pp} + J_{pp})\dot{n} = Q_E - Q_P - Q_f \end{cases} \quad (2)$$

where  $X_0$  and  $Y_0$  are the horizontal coordinates in the Earth coordinate system;  $\delta$  is the rudder angle;  $\psi$  is the heading angle;  $u$ ,  $v$ , and  $r$  are the translation and rotation speeds of the three degrees of freedom in the ship-following coordinate system;  $m$  is the ship mass;  $m_x$  and  $m_y$  are the wing sail-assisted ship additional masses in the  $G_x$ - and  $G_y$ -directions, respectively;  $I_{pp}$  and  $J_{pp}$  are the inertia moments and additional inertia moments of the propeller and the shafting; and  $I_{zz}$  and  $J_{zz}$  are the inertia moments and additional inertia moments corresponding to  $G_z$  in the ship-following coordinate system. Here, the influences on various parts of the ship are separately discussed. For example,  $X_H$  stands for the force exerted on the hull, dedicated to  $u$ , and  $X_P$  stands for the propeller.  $X_R$  stands for the rudder.  $X_W$  stands for environmental interference, and  $X_S$  stands for the wing sail. Similarly,  $Y_i$ , with  $i = H, R, S, W$ , represents the force dedicated to  $v$ , and  $N_i$  represents the turning torque  $r$ ;  $n$  is the speed of the propeller and the main engine;  $Q_E$  is the main-engine output torque;  $Q_P$  is the propeller torque; and  $Q_f$  is the torque consumed by the friction of the shafting.

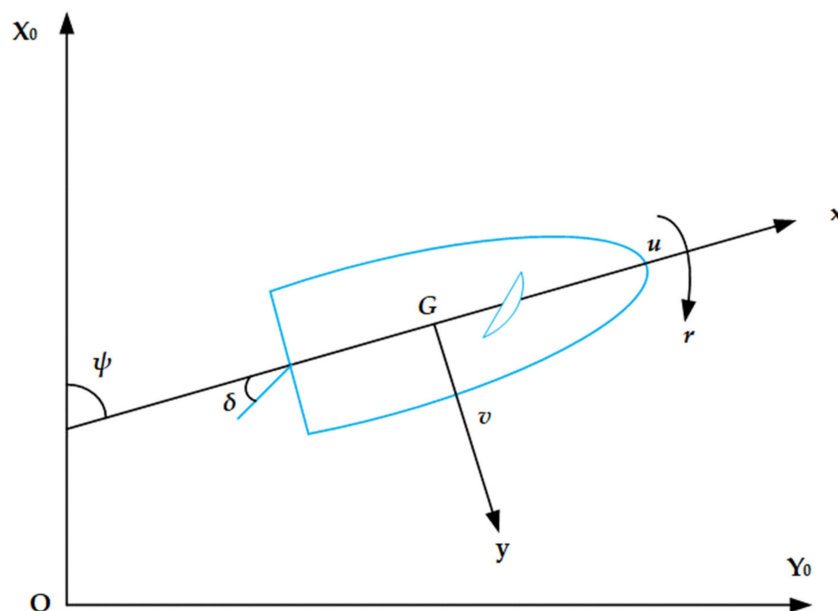


**Figure 2.** Ship motion coordinate system.

In this paper, only the relevant calculations of propeller thrust, rudder force, and wing force are expounded, and the other calculation formulas can be found in the literature [34], including complex fluid mechanics and mechanics.

The propeller thrust force and torque are calculated using Equation (3).

$$\begin{cases} X_P = (1 - t)\rho n^2 D^4 K_T \\ Q_P = \rho n^2 D^5 K_Q \end{cases} \quad (3)$$

where  $D$  is the propeller diameter;  $t$  is the thrust deduction coefficient;  $\rho$  is the density of seawater;  $n$  is the speed of the propeller; and  $K_T$  and  $K_Q$  are the propeller thrust and torque coefficients, which can be expressed as functions of the advance coefficient ( $J$ ). Equation (4) gives the formula of  $J$ .

$$J = u(1 - \omega)/nD \quad (4)$$

where  $J$  is the advance coefficient and  $\omega$  is the wake fraction.

The output power of the main engine,  $P_E$ , can be calculated according to Equation (5) as follows:

$$P_E = \frac{Q_E n}{9550} \quad (5)$$

The ship effective power can be calculated according to Equation (6) as follows:

$$P_H = \frac{P_E}{\eta_S \eta_O \eta_R \eta_H} \quad (6)$$

where  $P_H$  is the ship effective power when sailing,  $\eta_S$  is the shafting transmission efficiency,  $\eta_O$  is the propeller open water efficiency,  $\eta_R$  is the relative rotation efficiency, and  $\eta_H$  is the hull efficiency.

The hydrodynamic and torque models acting on the rudder are as follows:

$$\begin{cases} X_R = (1 - t_R) F_N \sin \delta \\ Y_R = (1 + \alpha_H) F_N \cos \delta \\ N_R = (x_R + \alpha_H x_H) F_N \cos \delta \end{cases} \quad (7)$$

where  $F_N$  is the perpendicular force on the rudder blade surface, as expressed in Equation (8);  $t_R$  is the deduction coefficient of the rudder blade resistance;  $\delta$  is the rudder angle;  $\alpha_H$  is the correction factor;  $x_H$  represents the  $x$  coordinate of the induced rudder force; and  $x_R$  is the  $x$  coordinate of the rudder in the ship-following coordinate system.

$$\begin{cases} F_N = -\frac{1}{2} \rho A_R f_a U_R^2 \sin \alpha_R \\ U_R = \sqrt{u_R^2 + v_R^2} \\ \alpha_R = \delta - \arctan \frac{v_R}{u_R} \end{cases} \quad (8)$$

where  $A_R$  is the rudder blade area;  $U_R$  is the effective velocity at the rudder blade;  $v_R$  is the effective transverse velocity;  $u_R$  is the effective longitudinal velocity; and  $\alpha_R$  is the effective angle of attack relative to the rudder blade.

## 2.2. Wing Sail Force Analysis

The wing force can be expressed by the following equation:

$$\begin{cases} X_W = 0.5 C_X \rho_a V_a^2 S_W \\ Y_W = 0.5 C_Y \rho_a V_a^2 S_W \\ N_W = Y_W x_S \end{cases} \quad (9)$$

where  $C_X$  and  $C_Y$  are the thrust and lateral thrust coefficients,  $\rho_a$  is the air density,  $S_W$  is the wing sail projected area, and  $x_S$  is the longitudinal distance from the point where  $Y_W$  acts to the center of gravity of the ship.

The thrust of the wing is the result of the combination of lift and drag forces. As shown in Figure 3,  $C_L$  and  $C_D$  are the lift and drag coefficients of the wing sail; when a line is vertical to the ship course line, which passes through the coordinate origin and is tangent to the curves of  $C_L$  and  $C_D$ , tangent point A ( $C_{LA}$ ,  $C_{DA}$ ) has the largest thrust coefficient, and the corresponding angle of attack is the best angle of attack for wing sails at this wind direction angle. The relationship among  $C_X$ ,  $C_Y$ ,  $C_L$ , and  $C_D$  can be expressed as shown in Equation (10).

$$\begin{cases} C_X = C_L \sin \beta - C_D \cos \beta \\ C_Y = C_L \cos \beta + C_D \sin \beta \end{cases} \quad (10)$$

where  $\beta$  is the relative wind direction angle.

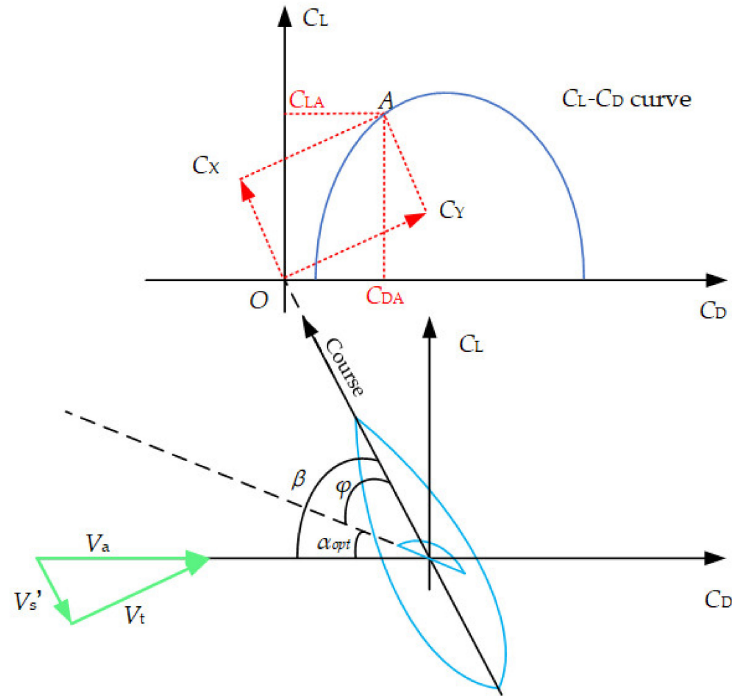


**Figure 3.** Force analysis of wing sails.

In addition, the relationship among the relative wind direction angle ( $\beta$ ), the best attack angle of the wing sail ( $\alpha_{opt}$ ), and the turning angle of the wing sail ( $\varphi$ ) is shown in Equation (11).

$$\varphi = \beta - \alpha_{opt} \quad (11)$$

When  $\beta$  is determined, the wing sail can work at the best attack angle by controlling the wing sail turning angle, and the best thrust effect can be obtained.

$C_L$  and  $C_D$  are determined by the aerodynamic characteristics of the wing sail. The coordinate system was established for the U-shaped wing sail in the wind tunnel test, as shown in Figure 4.

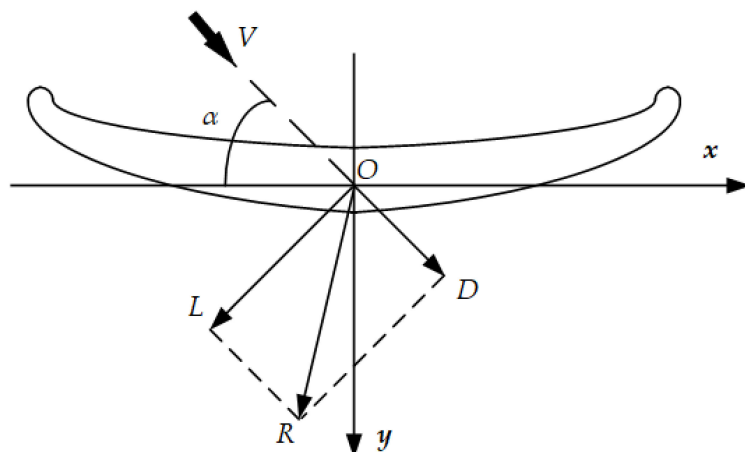


**Figure 4.** U-shaped wing coordinate system and force analysis.

$C_L$  and  $C_D$  are calculated according to Equation (12).

$$\begin{cases} C_L = L / 0.5 \rho_a V^2 S_m \\ C_D = D / 0.5 \rho_a V^2 S_m \end{cases} \quad (12)$$

where  $L$  and  $D$  are the wing sail model lift and drag,  $S_m$  is the area of the wing sail model, and  $V$  is the wind speed in the wind tunnel test.

Considering the stability of the ship course, it is necessary to adjust the rudder angle to compensate for the lateral thrust of the wing sail. The ship course is also affected by environmental factors; the adjustment of the rudder to keep the ship sailing on the preset course is realized with the automatic control of the autopilot during the sailing process. The corresponding rudder angle is calculated according to Equations (7) and (9), and the net thrust of the wing sail can be obtained by subtracting the resistance caused by the increase in the rudder angle from the thrust of the wing sail.

### 2.3. Wind Resource Analysis Method

To realize the characteristic analysis of wind resources, the wind field data of the sailing area are essential. The wind field data in this paper came from the fifth reanalysis data (ERA5) of European Centre for Medium-Range Weather Forecasts (ECMWF). The wind field information on the sailing route was extracted using the spatial and temporal interpolation method as follows:

Step 1. Determine the target sea area and download the dataset in the target sea area.

Step 2. Read the time, longitude, latitude, and wind field information data in the dataset.

Step 3. Take the latitude and longitude of the route and time as reference quantities, and extract the wind field data from the dataset.

Step 4. Check whether the coordinate time of the route is an integer multiple of 6 h. If it is, at the integer time point, carry out two-dimensional surface interpolation to extract the wind field data of the current coordinate point.

Step 5. If the coordinate time is not on the integer time node, read the adjacent time data before and after the target time; then, interpolate them with the target time. The extracted datum is a one-dimensional vector, and each element is the wind field information of the corresponding coordinates on the sailing route.

As the wind field data from ECMWF are for true wind, it is necessary to calculate the relative wind field considering the speed and course of ships. The definition of relative wind direction is in Figure 5.

The relative wind field calculation method is shown in Figure 6. The extracted wind field data of the sailing route and the wind caused by ship motion are decomposed in the u- and v-directions; then, the relative wind field is calculated.

In the figure,  $V_S'$  is the wind caused by ship motion,  $V_t$  is the true wind, and  $V_a$  is the relative wind.  $u$  and  $v$  are the longitude and latitude directions.

The wind field probability matrix of the sailing route was obtained by referring to the format of IMO MEPC. 1/Circ. 896 after calculating the relative wind field, as shown in Table 1.

In the matrix, each row represents the wind speed range; for example, <1 represents [0,1), <2 represents [1,2)... <25 represents [24,25), and  $\geq 25$  represents [25,  $\infty$ ). Each column represents the wind direction angle interval; for example, 0 represents [0, 5), 5 represents [5, 10)... 355 represents [355,360). Further, each element represents the wind field probability within the wind speed and direction range. For example,  $W_{3,2}$  represents the probability value of wind speed of [2–3] m/s and wind direction angle in the range of [5–10] $^\circ$ . The sum of all elements in the matrix is 1.

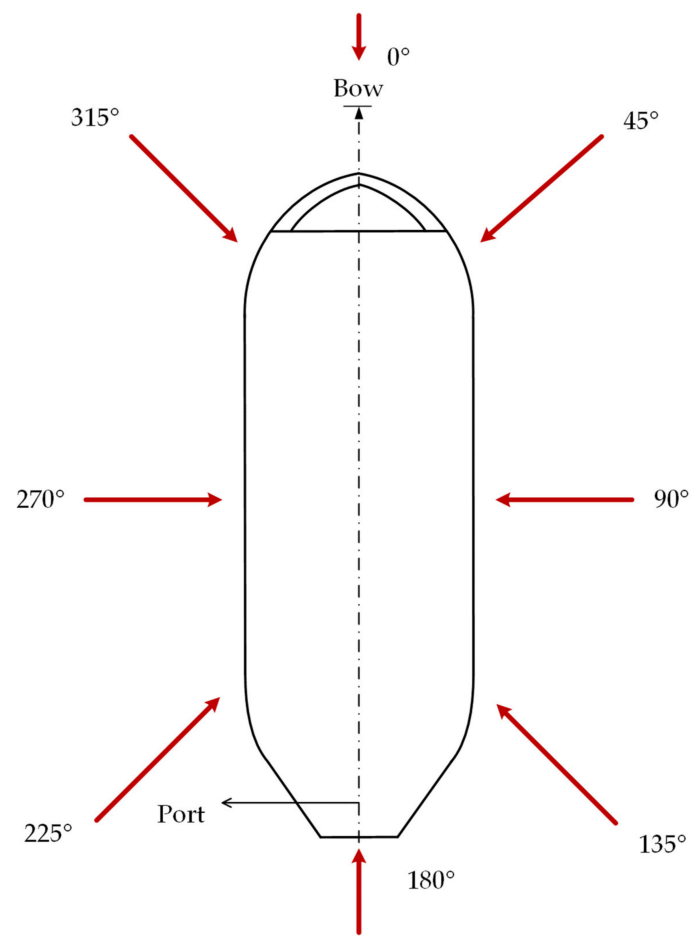


**Figure 5.** Definition of wind direction relative to ships.

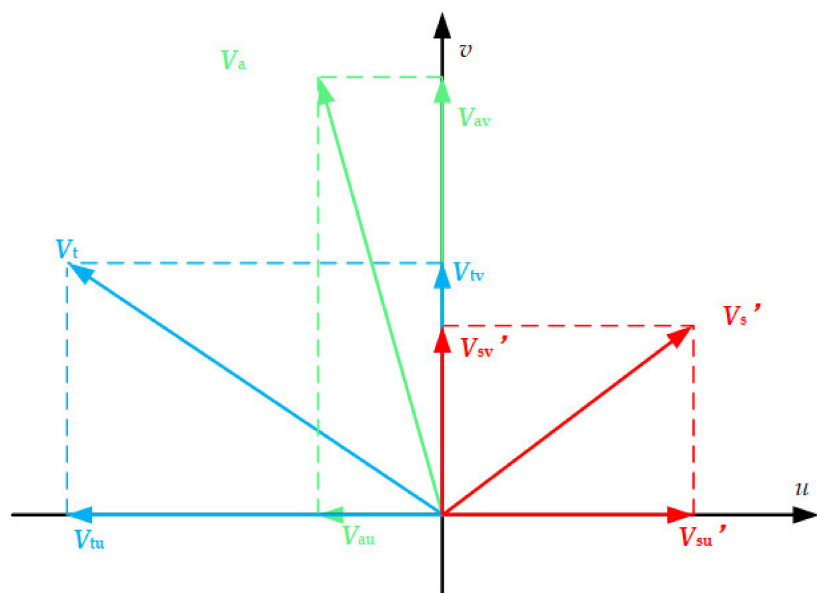


**Figure 6.** Calculation method of relative wind field.

**Table 1.** Layout of the wind field probability matrix.

Wind Speed (m/s) \ Wind Angle (°)	0	5	...	355
<1	W <sub>1,1</sub>	W <sub>1,2</sub>	...	W <sub>1,72</sub>
<2	W <sub>2,1</sub>	W <sub>2,2</sub>	...	W <sub>2,72</sub>
<3	W <sub>3,1</sub>	W <sub>3,2</sub>	...	W <sub>3,72</sub>
:	:	:	...	:
<25	W <sub>25,1</sub>	W <sub>25,2</sub>	...	W <sub>25,72</sub>
≥25	W <sub>26,1</sub>	W <sub>26,2</sub>	...	W <sub>26,72</sub>

#### 2.4. Evaluation Method for Energy Saving of Wing Sail

According to the wind field probability matrix and Equation (9), the wing sail thrust force matrix for the sailing route was calculated according to the below principles.

Wind speed takes the upper limit of each interval, and wind direction takes the middle value of each interval. According to the control strategy of wing sails, the wing sail does not work when the wind speed is over 25 m/s, considering the safety of ships; therefore, the wind speed of the last row was calculated as 25 m/s. The thrust force matrix is shown in Table 2.

**Table 2.** Layout of the thrust force matrix of wing sails.

Wind Speed (m/s) \ Wind Angle (°)	2.5	7.5	...	357.5
1	F <sub>1,1</sub>	F <sub>1,2</sub>	...	F <sub>1,72</sub>
2	F <sub>2,1</sub>	F <sub>2,2</sub>	...	F <sub>2,72</sub>
3	F <sub>3,1</sub>	F <sub>3,2</sub>	...	F <sub>3,72</sub>
:	:	:	...	:
25	F <sub>25,1</sub>	F <sub>25,2</sub>	...	F <sub>25,72</sub>
25	F <sub>26,1</sub>	F <sub>26,2</sub>	...	F <sub>26,72</sub>

In the matrix, the elements represent the thrust of the wing sail in the corresponding wind speed and direction angle range. For example, F<sub>3,2</sub> represents the thrust force generated by the wing sail at the relative wind speed of 3 m/s and the relative wind direction angle of 7.5°.

The total thrust ( $F_M$ ) of the wing sail is the sum of all elements in the thrust force matrix, and the thrust power of the wing sail on the sailing route can be calculated with Equation (13).

$$P_W = \sum_{i=1}^{26} \sum_{j=1}^{72} F_{i,j} V_S \quad (13)$$

where  $P_W$  is the propulsion power provided by the wing sail on the sailing route, and  $i$  and  $j$  are the indexes of the thrust force matrix, with  $i = 1, 2, \dots, 26$  and  $j = 1, 2, \dots, 72$ .

Equation (14) gives the calculation of the wing sail energy-saving effect.

$$\eta_W = \frac{P_W}{P_H} \quad (14)$$

where  $\eta_W$  is the wing sail energy-saving effect on the sailing route and  $P_H$  is the ship effective power when sailing.

The wind wing energy-saving evaluation process is summarized in Figure 7.

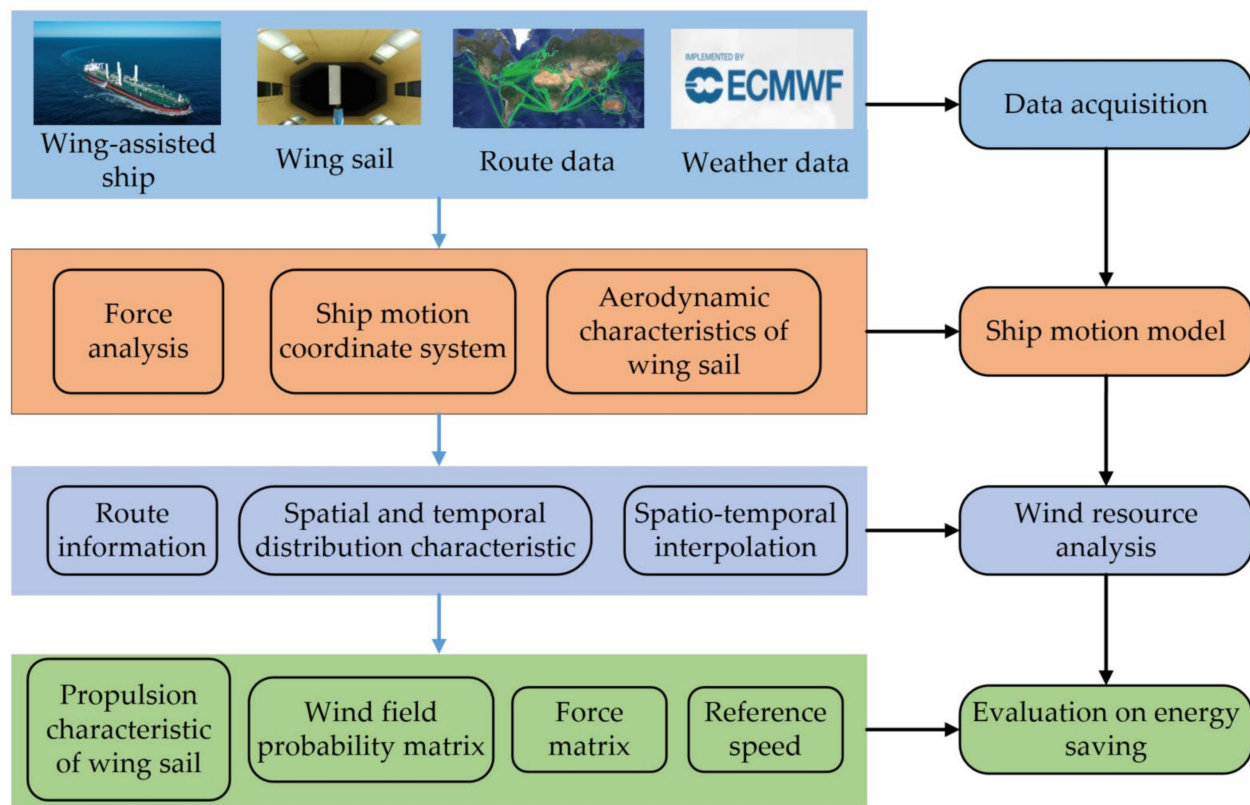


**Figure 7.** Energy-saving evaluation process of wing sail-assisted ships.

Firstly, the research object and data such as ship parameters, and route and wind information are obtained.

Then, a ship motion model, which is used to calculate the effective power of ships, is established using ship force analysis and ship motion coordinate transformation.

The distribution characteristics of the wind field in the sailing area are obtained by analyzing and reconstructing the meteorological data of the global sea.

Finally, the wind field probability matrix for the ship route is constructed; the thrust power of the wing sail is calculated; and the evaluation of the energy-saving effect is realized.

### 3. Case Study

#### 3.1. Study Object

A wing sail-assisted VLCC that sailed on the China-to-Middle East route was chosen as the target ship, and its principal dimensions are shown in Table 3.

**Table 3.** Principal dimensions of target ship.

Dimension	Value
Overall length	332.95 m
Length between perpendiculars	323.60 m
Breadth	60.00 m
Depth	30.00 m
Design draft	20.50 m
Structural draft	21.80 m
Camber	1.50 m

The position and arrangement of the sails have an influence on the energy-saving effect. In ships with the center of transverse resistance located at the bow, the wind propulsion system is usually only applicable to the position where the center of aerodynamic pressure is also located near the bow. Alternatively, the installed wind propulsion system should be kept small enough to keep the side forces and rudder angle quite small. The target ship was equipped with two pairs of wing sails on the main deck. After considering the factors of the bridge visibility requirement of International Convention for Safety of Life at Sea (SOLAS), the ship structural strength, and the ship stability, the wing sails were symmetrically arranged at port and starboard, and their number and positions are shown in Figure 8.



**Figure 8.** Target ship and wing sail positions.

The coordinates of each wing sail are illustrated as follows: the first number is the distance between the wing sail and the stern, and the second number is the distance between the wing sail and midship, which is positive when port and negative when starboard.

Table 4 shows the parameters of the wing sails.

**Table 4.** Parameters of wing sails.

Parameter	Value
Overall height	39.68 m
Width	14.80 m
Wing height	35.60 m
Mast height	37.40 m
Base height	2.27 m
Number of sections	3
Number of wing sails	4

The mathematical model of the target ship was established according to Section 2. The main-engine output power at different speeds was calculated and compared with the trial report of the target ship, as shown in Table 5.

**Table 5.** Trial and simulation results of main-engine power.

Percentage of Design Speed	Speed (kn)	Trial Report (kW)	Model (kW)	Deviation
100%	15.7	18,270.0	18,266.4	-0.02%
95%	14.9	15,670.0	15,530.4	-0.89%
90%	14.2	13,350.0	13,454.5	0.78%
85%	13.4	11,270.0	11,393.2	1.09%
80%	12.6	9450.0	9561.1	1.18%
75%	11.8	7840.0	7746.6	1.19%
70%	11.0	6430.0	6475.7	0.71%
65%	10.2	5210.0	5144.7	-1.25%

The deviations between model and trial report were within 1.25% at different speeds, indicating that the established ship motion model was effective and could be used to calculate the power of the target ship.

According to the U-shaped wing sail wind tunnel test equipment on the target ship, the lift and drag coefficients at different attack angles are shown in Figures 9 and 10.

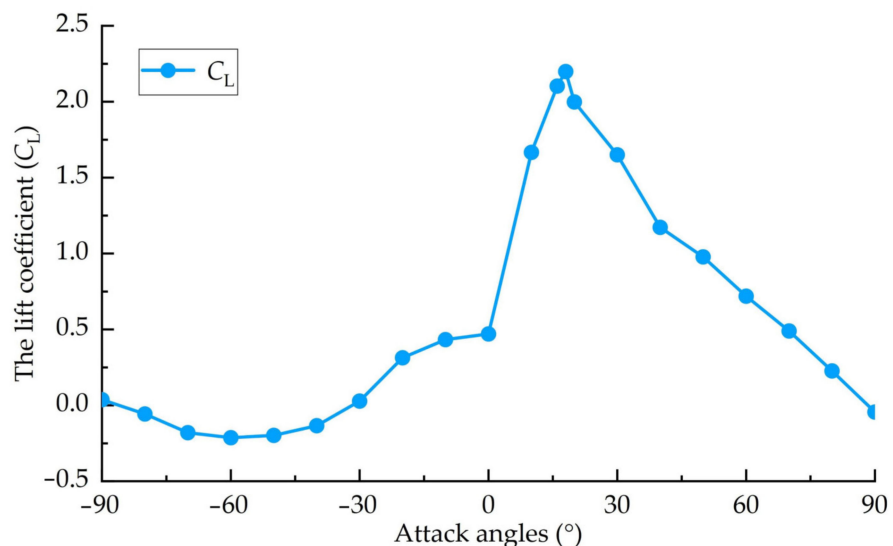


**Figure 9.** Lift coefficient at different attack angles.

In Figure 9, the lift coefficient of the wing sail is negative in the range of  $-90^\circ$  to  $-30^\circ$ , and it increases in the range of  $-30^\circ$  to  $18^\circ$ . The lift coefficient reaches the maximum value of 2.199 at the position of  $18^\circ$ ; then, it decreases as the attack angle increases. The lift coefficient greatly varies before and after the attack angle of  $0^\circ$ ; the reason is that the convex and concave shapes of the wing sails are different. When the attack angle is in the range of  $-90^\circ$  to  $0^\circ$ , the wind comes from the convex surface of the wing sail, while the wind comes from the concave surface in the  $0^\circ$ -to- $90^\circ$  range. The attack angle of  $18^\circ$  is where the maximum lift coefficient occurs; then, with the increase in the attack angle, more and more vortex and boundary layer separation form on the back pressure surface of the wing sail, leading to the gradual decrease in the lift coefficient within the attack angle range of  $30^\circ$  to  $90^\circ$ .

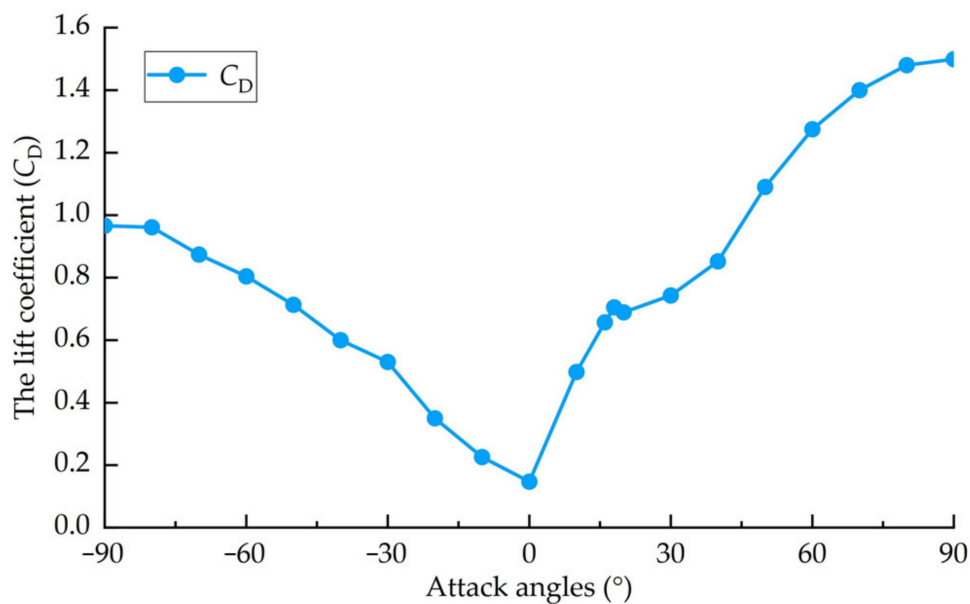


**Figure 10.** Drag coefficient at different attack angles.

In Figure 10, the drag coefficient of the wing sail decreases as the attack angle increases in the range of  $-90^\circ$  to  $0^\circ$ , and the drag coefficient increases in the angle range of  $0^\circ$  to  $90^\circ$ . Obviously, as the wing sail rotates, the drag coefficient increases as the wing sail projected area along the wind direction increases.

According to the parameters of the wing sails and the analysis in Section 2.2, the relationship between the thrust force and the relative wind direction angle of the target wing sails at unit wind speed (1 m/s) is shown in Figure 11.

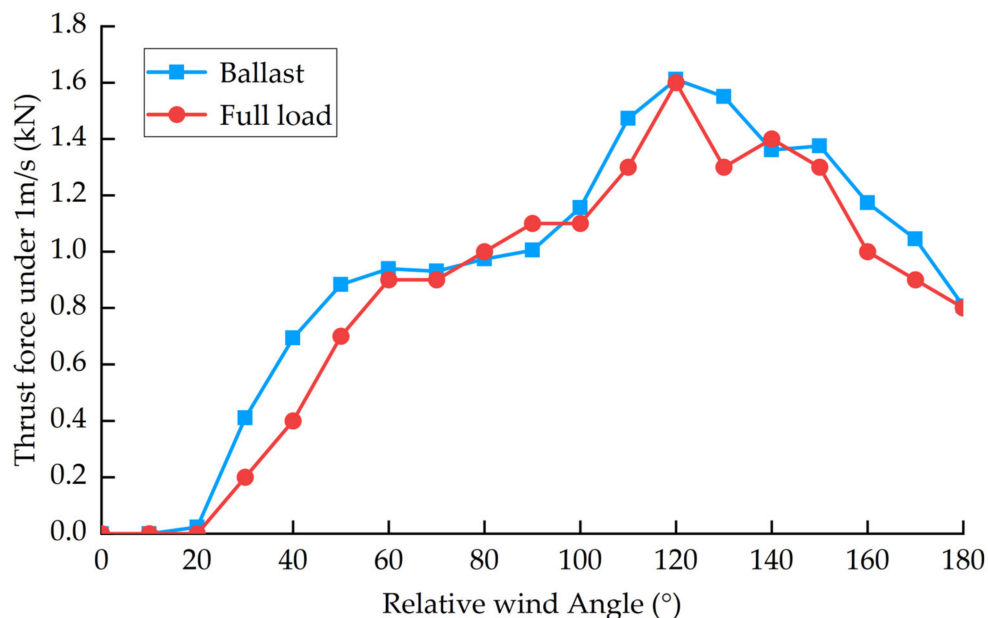


**Figure 11.** Thrust force of wing sail at different relative wind angles.

According to Figure 11, the thrust force under the ballast condition is larger than that under the full-load condition in most relative wind angle ranges. The reason is that the draft under the ballast condition is smaller than that under the full-load condition, which means that the wing sail under the ballast condition is higher than that under the full-load condition with respect to the sea surface and has higher wind speed under the

ballast condition. Due to the different interference effects between the wing sails and the ship superstructure under the two loading conditions, the thrust force under the full-load condition is larger than that under the ballast condition when the relative wind angle is from  $80^\circ$  to  $95^\circ$ , as well as around  $140^\circ$ . The range of 0-to- $15^\circ$  relative direction angles does not produce thrusting force, which is an invalid range for wing sails. Due to the symmetrical structure of wing sails, an invalid range also appears at  $345^\circ$ -to- $360^\circ$  relative direction angles.

### 3.2. Analysis of Wind Resources on Target Route

The target ship usually sailed from China ( $121.84^\circ$  E,  $29.94^\circ$  N) to the Middle East ( $47.93^\circ$  E,  $29.35^\circ$  N) in ballast condition and sailed back to China in full-load condition, and the service speeds were 12.5 kn and 12 kn, respectively. It took the ship approximately one month to complete one single voyage, and a year for six round voyages. The target route is shown in Figure 12.

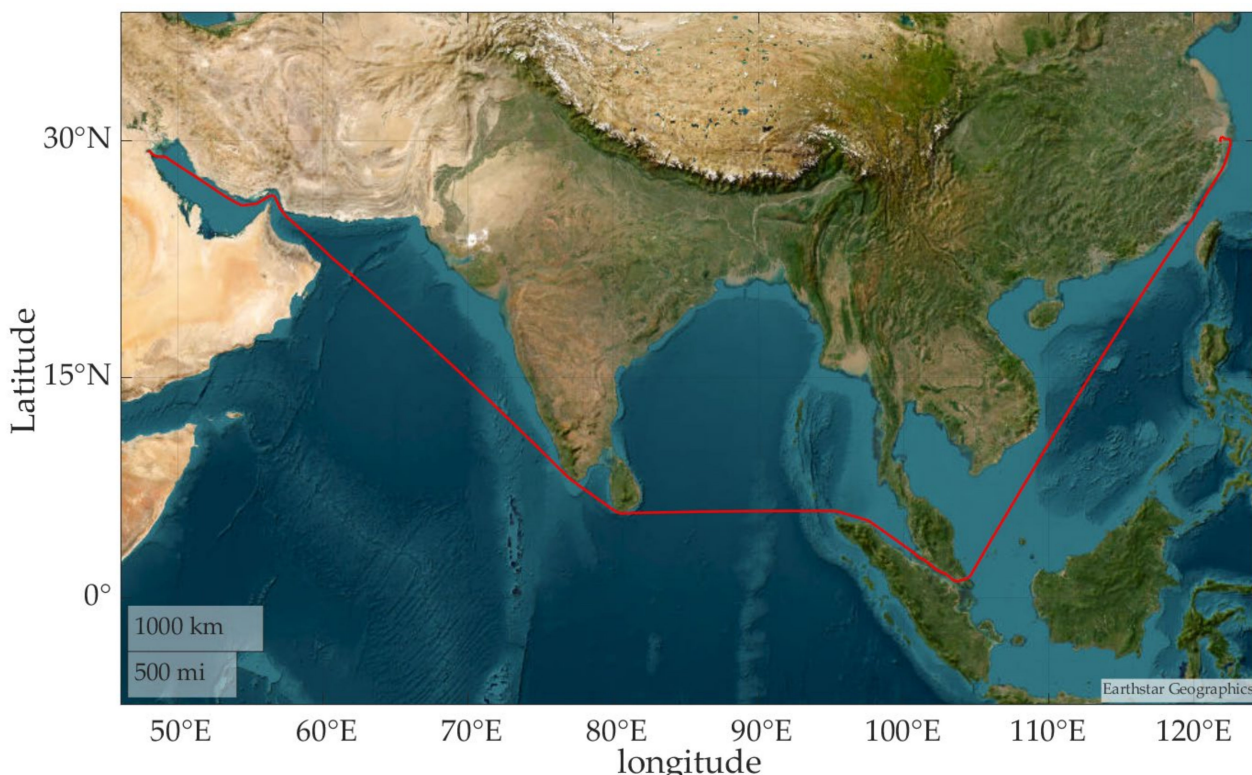


**Figure 12.** Target route.

The target ship sailed through the Arabian Sea, the Bay of Bengal, and the South China Sea. The global wind field data released by ECMWF in 2021 were used for wind resource analysis and energy-saving evaluation.

The spatial-temporal analysis of the wind field in the Bay of Bengal that the target route passed through is shown in Figures 13 and 14, respectively (the red line in the figure is part of the target route).

According to Figure 13, the highest wind speed was 11.5 m/s, which occurred in August, and the lowest wind speed was 1.5 m/s in June. The mean wind speed in August was higher than that in other months. According to Figure 14, the wind directions in April, June, August, September, and October were distributed within  $90^\circ$  and were lower than those in other months. Both wind speed and direction significantly varied in different months.

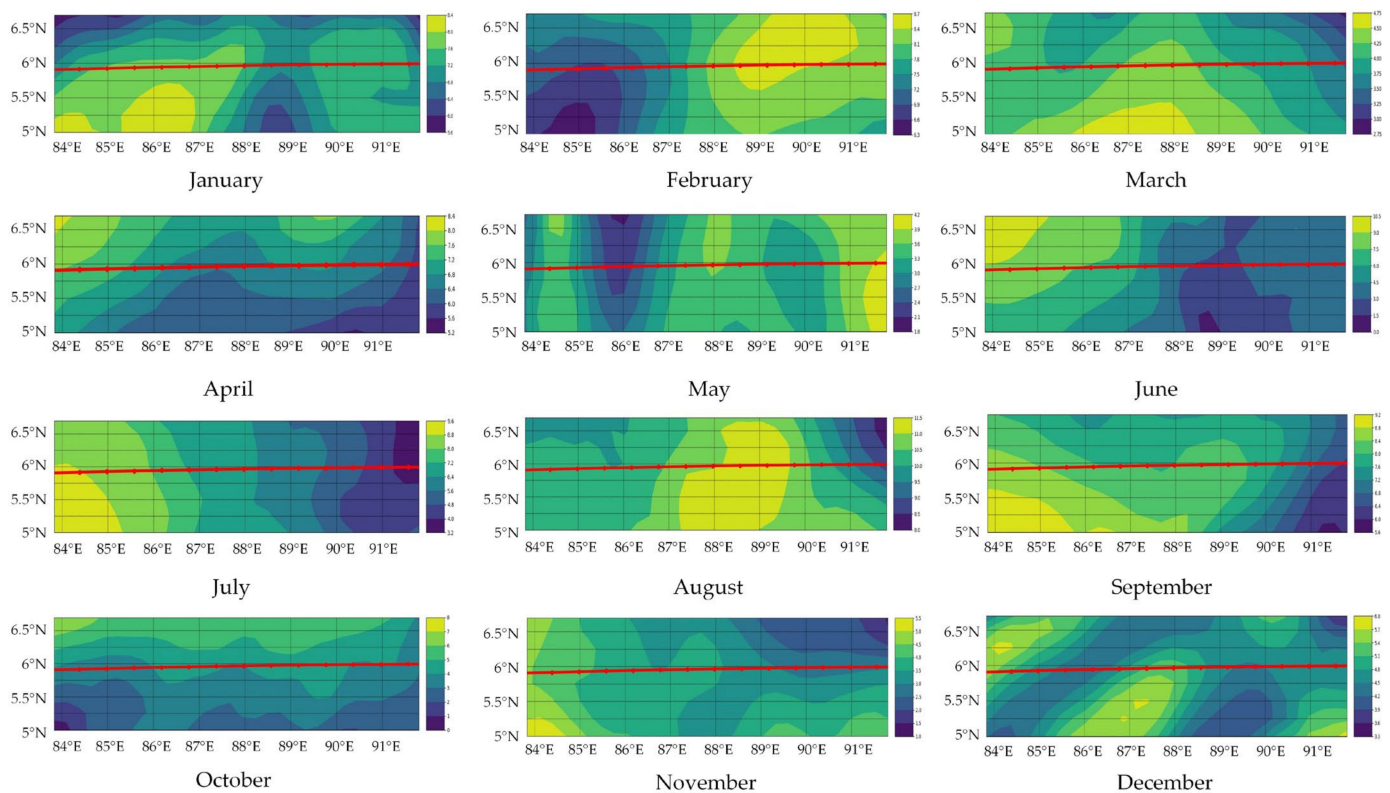


**Figure 13.** Spatial–temporal distribution characteristics of wind speed in Bay of Bengal.

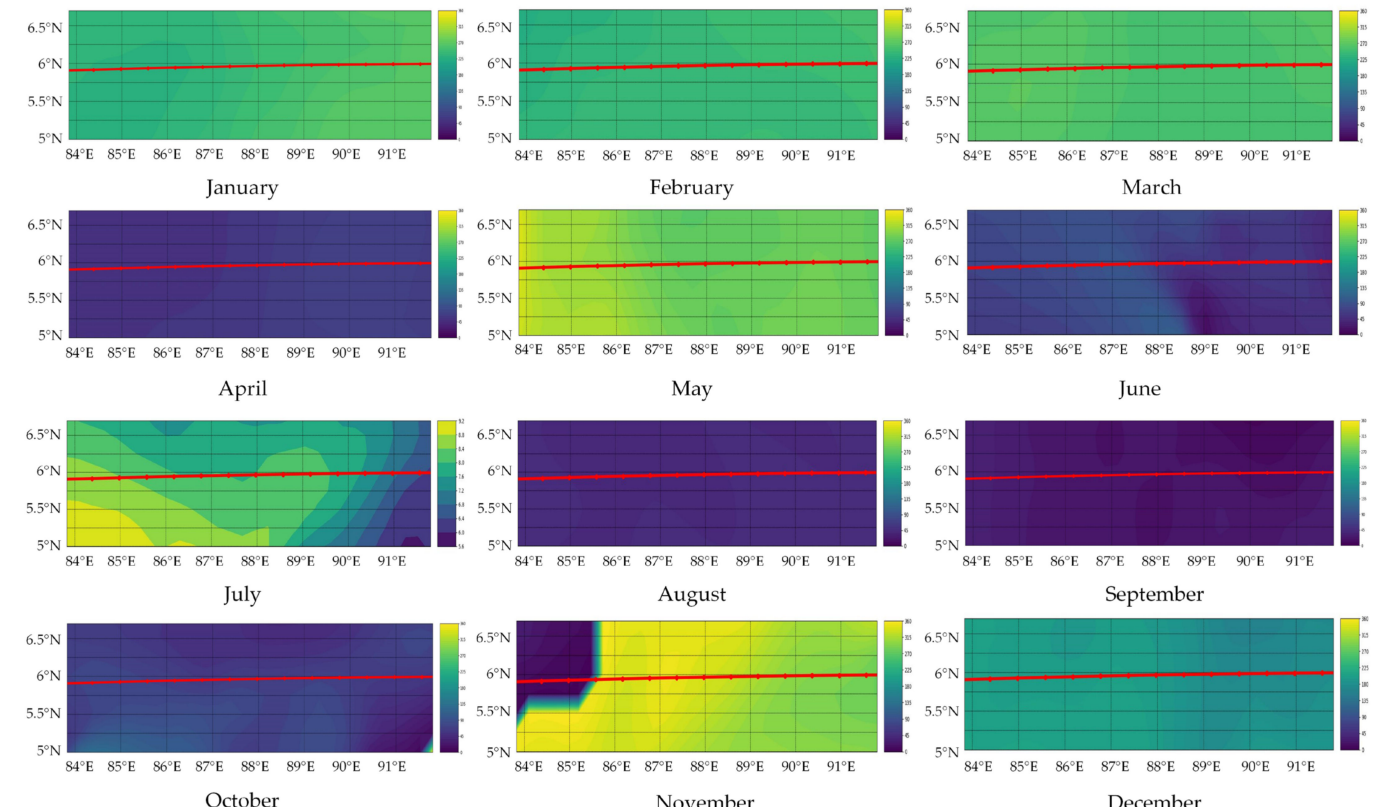


**Figure 14.** Spatial–temporal distribution characteristics of wind direction angle in Bay of Bengal.

The wind rose more clearly represents the distribution characteristics of wind, as shown in Figure 15. The wind in April, May, June, November, and December was distributed in a more disperse manner than in other months. Knowing the distribution characteristics of wind on the target sailing route, the best thrust effect could be achieved by adjusting the turning angle of the wing sails.

Wind resource information on the Arabian Sea and South China Sea are in Supplementary Materials. Figures S1 and S2 show the spatial-temporal distribution characteristics of wind speed and direction in the Arabian Sea, and Figure S3 shows the wind rose in the Arabian Sea. Figures S4 and S5 show the spatial-temporal distribution characteristics of wind speed and direction in the South China Sea, and Figure S6 shows the wind rose in the South China Sea. The wind also showed spatial-temporal difference distribution characteristics in the Arabian Sea and South China Sea.

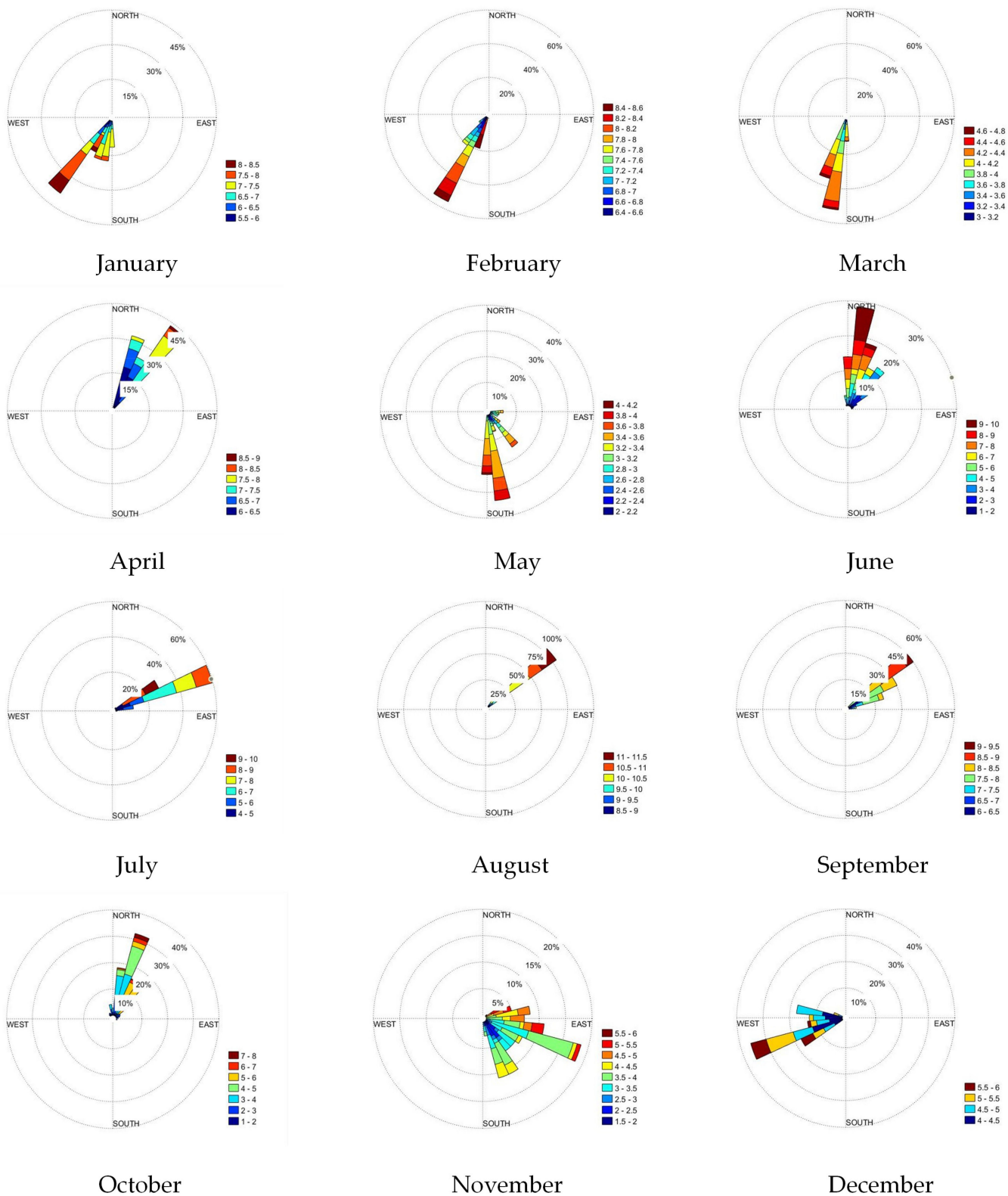
The monthly wind field probability matrix for the target route was constructed according to the method introduced in Section 2.3. As the matrix data are too many to be displayed in tables, this paper shows and explains the wind field probability matrix for the target ship in ballast condition in January in the form of pictures. As shown in Figure 16, the depth of the yellow color indicates the probability value of the matrix, that is, the deeper the yellow color is, the greater the probability is. Some key data in the matrix (red box area) are enlarged to display the values. The wind field probability matrix data are in Supplementary Materials Files S1 and S2. File S1 gives the wind field probability matrix under the ballast condition on the target route in 2021, and File S2 gives the wind field probability matrix under the full-load condition on the target route in 2021.

According to Figure 16, the highest probability, which was 0.00893, occurred at 9 m/s and 355° of relative wind during ballast sailing in January, and the relative wind field was concentrated in the wind speed range of 7–13 m/s and the wind direction range of 335–355°, as well as 0–10°.

The wind field data within the invalid range of target wing sails were excluded from the wind field probability matrix, and the total amount of remaining available wind resources was calculated to obtain the level of available wind resources on the routes in the corresponding months, as shown in Table 6. The highest level of available wind resources under ballast condition was 66.4% in July. The highest level of available wind resources under full-load condition was 72.8% in January. The lowest level of available wind resources in the whole year under ballast and full-load conditions were 48.9% and 53% in May and June, respectively.

**Table 6.** Monthly levels of available wind resources on target route in 2021.

Month	Level of Available Wind Resources (Ballast Condition)	Level of Available Wind Resources (Full-Load Condition)
January	55.9%	72.8%
February	59.8%	70.0%
March	57.3%	64.2%
April	54.0%	53.1%
May	48.9%	53.0%
June	48.9%	53.0%
July	66.4%	65.9%
August	63.4%	62.4%
September	58.5%	59.9%
October	55.5%	62.2%
November	55.5%	58.0%
December	59.5%	68.1%

**Figure 15.** Wind rose in Bay of Bengal.

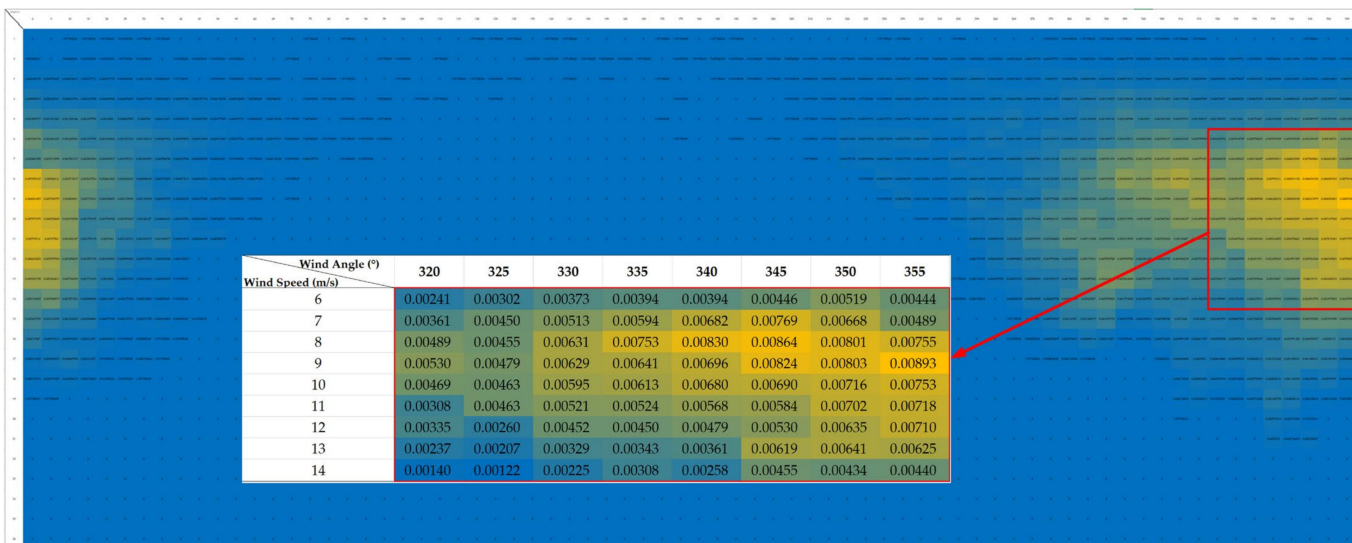


**Figure 16.** Wind field probability matrix under ballast condition on target route in January.

The wind thrust force matrix can be constructed by multiplying the wind field probability matrix by the thrust of the wing sails at the corresponding wind speed and direction. The wind thrust force matrix under the ballast condition on the target route in January is shown in Figure 17. The wind field thrust force matrix data are in Supplementary Materials Files S3 and S4. File S3 gives the thrust force matrix under the ballast condition on the target route in 2021, and File S4 gives the thrust force matrix under the full-load condition on the target route in 2021.

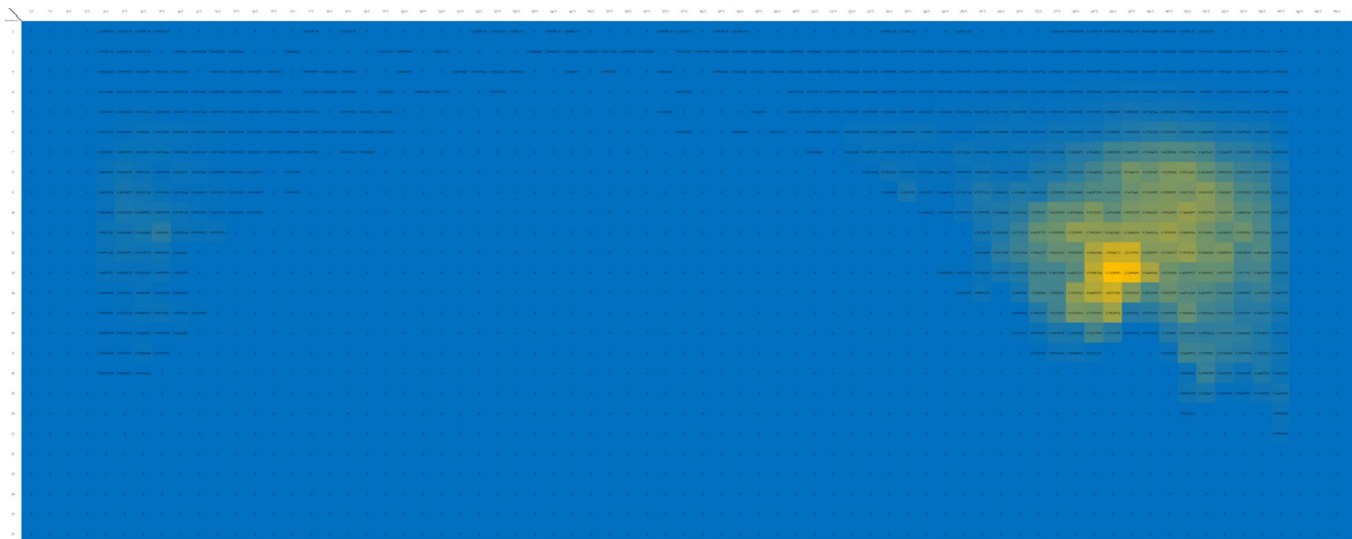


**Figure 17.** Thrust force matrix under ballast condition on target route in January.

According to Figure 17, the thrust characteristics of the wing sails changed the matrix distribution of the wind field probability matrix and provided greater thrust force in the range of relative wind speed of 10–15 m/s and relative wind direction of 210–320°. We summed all the data in the thrust force matrix to obtain the total propulsion force of the wing sail on the target route and calculated the propulsion power of the wing sails according to Equation (13). The total thrust force of the target ship in January was 74.2 kN; the speed of the target ship in ballast condition was 12.5 kn; and the wing propulsion power was 477.15 kW.

### 3.3. Results and Discussion

The service speed of the target ship in ballast condition was 12.5 kn, and it was 12.0 kn in full-load condition. According to the established mathematical model of ship motion, the corresponding mean effective power values of the ship were calculated to be 5290 kW in ballast condition and 7000 kW in full-load condition. The monthly energy-saving effect of the target ship on the target route was calculated according to Equations (13) and (14), as shown in Table 7.

**Table 7.** Energy-saving effect of wing sails on target route.

Month	Ballast Condition (12.5 kn; 5290 kW)			Full-Load Condition (12.0 kn; 7000 kW)		
	Thrust (kN)	Propulsion Power (kW)	Energy-Saving Effect	Thrust (kN)	Propulsion Power (kW)	Energy-Saving Effect
January	74.20	477.15	9.02%	66.96	413.37	5.91%
February	66.22	425.83	8.05%	54.60	337.06	4.82%
March	53.87	346.41	6.55%	43.04	265.70	3.80%
April	39.56	254.39	4.81%	29.77	183.78	2.63%
May	37.44	240.76	4.55%	27.47	169.58	2.42%
June	37.44	240.76	4.55%	27.47	169.58	2.42%
July	78.46	504.54	9.54%	58.97	364.04	5.20%
August	58.46	375.93	7.11%	43.23	266.87	3.81%
September	46.59	299.60	5.66%	33.31	205.63	2.94%
October	57.14	367.44	6.95%	48.33	298.36	4.26%
November	54.34	349.44	6.61%	43.29	267.24	3.82%
December	75.56	485.89	9.19%	65.23	402.69	5.75%

According to Table 7, the energy-saving effect of the wing sails was the lowest in May and June under both sailing conditions, i.e., 4.55% under the ballast condition and 2.42% under the full-load condition. This was caused by the dispersed distribution of wind and low relative wind speed in May and June, which is consistent with the results of the wind resource analysis in Section 3.2. Under the ballast condition, the wing sails provided the highest energy-saving effect in July, 9.54%, and the highest energy-saving effect under the full-load condition was 5.91% in January. This means that the fuel consumption and carbon emissions of ships could be effectively reduced using wing sails.

In addition, the energy-saving effect under the ballast condition was better than that under the full-load condition each month under the same true wind field. The first reason is that the difference in ship speed and course led to the change in the relative wind field, which in turn changed the thrust force matrix of the wing sails. The second reason is that the effective power of the ship in ballast condition was much lower than that in full-load condition, and the energy-saving effect under the ballast condition was better even with the same propulsion power of the wing sails.

There were two sailing plans for six round voyages of the target ship in one year. Plan A: Ballast sailing in odd months and full-load sailing in even months; an annual energy-saving effect of 5.47% could be achieved in this scenario. Plan B: Ballast sailing in even months and full-load sailing in odd months; an annual energy-saving effect of 5.39% could be achieved in this scenario.

The sailing area and the environment conditions constantly change due to the adjustment of ship speed and course during the sailing process. The wind field probability matrix was constructed to analyze the distribution characteristics of wind resources. On this basis, the energy-saving evaluation of wing sails was realized by calculating the wing sail thrust force and ship effective power according to the ship motion model. The energy-saving evaluation method proposed in this paper is not limited to specific types of ships, and the

data needed for this method are not complex compared with empirical formulas and the computational fluid dynamics analysis method; thus, it has the advantage in general applicability. Therefore, the proposed method in this paper can provide reference for shipping companies to make ship sailing plans, and with reasonable planning, the energy-saving effect of wing sails could be further improved to reduce the carbon emission of ships.

Nevertheless, there are also some factors that should be considered for the use of wing sails. The installation of wing sails on deck could adversely affect visibility from the bridge; thus, duty officers should be more careful when performing lookout work. Wing sails, along with lifting, lowering, and slewing equipment, need routine maintenance and repair in case of failure, which could lead to extra maintenance costs. The design and installation of wing sails cause additional costs when compared with regular ships. These factors should be considered by the shipping company when performing economic analyses.

#### 4. Conclusions

Effective methods for the evaluation of energy saving can provide guidance for the popularization and application of sail-assisted technology, as well as the improvement of the wind energy utilization efficiency of ships. To fully tap the marine wind energy utilization potential of ships, an energy-saving evaluation method for sail-assisted ships based on the wind resource analysis of the shipping route is proposed. Firstly, a ship motion model considering wing sail force is established, and the influence of wing sail lateral force on the ship is balanced using the rudder force module. Then, by analyzing the spatial-temporal distribution characteristics of the wind field in the sea area where ships sail, a wind resource analysis method based on spatial-temporal interpolation is proposed to calculate the level of available wind resources on ship routes. Finally, based on the thrust matrix of the wing sails and the sailing condition, a method for the calculation of the energy-saving effect of wing sail-assisted ships is proposed. A case study of a VLCC shows that marine wind resources change greatly in time and space. The available wind resources of the target ship varied from 48.9% to 72.8% each month in 2021, and the corresponding energy-saving effect also varied from 2.42% to 9.54%. An annual energy-saving effect of 5.47% could be achieved with the reasonable design of the ship sailing plan. Furthermore, the energy-saving effect could be further improved if more than four wings were adopted. This could greatly reduce the fuel cost of ships and improve the competitiveness of shipping companies on the market. In addition, the proposed method only requires wind resource data and ship sailing information and is not limited to specific types of ships. Therefore, the method has general applicability, could be applied to any ship and route suitable for the use of wing sails, and could provide decision-making reference for shipping companies to make fleet navigation plans to promote the development of low-carbon shipping.

In this paper, the interrelated interference among wing sails was not considered, and this may have resulted in an attenuation effect on the wing sail thrust force; interference among wing sails in ships smaller than a VLCC is expected to be considerable, which should be further considered in future work. Meanwhile, more factors, such as daily fluctuations in wind strength caused by temperature change and the influence of ocean currents on ship motion, should be comprehensively considered in further research to make the evaluation method more effective. Additionally, research on energy-saving evaluation systems for wing sail-assisted ships on global trade routes will be carried out based on the proposed method to further improve the potential of emission reduction in the shipping industry using wind energy.

**Supplementary Materials:** The following supporting information can be downloaded at: <https://www.mdpi.com/article/10.3390/jmse11040789/s1>, Figure S1: Spatial-temporal distribution characteristics of wind speed in Arabian Sea, Figure S2: Spatial-temporal distribution characteristics of wind direction angle in Arabian Sea, Figure S3: Wind rose in Arabian Sea, Figure S4: Spatial-temporal distribution characteristics of wind speed in South China Sea, Figure S5: Spatial-temporal distribution characteristics of wind direction angle in South China Sea, Figure S6: Wind rose in South China Sea, File S1: Wind field probability matrix under ballast condition on target route in 2021, File S2: Wind

field probability matrix under full-load condition on target route in 2021, File S3: Thrust force matrix under ballast condition on target route in 2021, File S4: Thrust force matrix under full-load condition on target route in 2021.

**Author Contributions:** Conceptualization, R.M.; methodology, R.M. and Z.W.; software, R.M., Z.W. and H.Z.; validation, R.M. and H.Z.; investigation, B.J. and Y.L.; resources, R.M. and L.H.; writing—original draft preparation, R.M. and Z.W.; writing—review and editing, R.M.; visualization, R.M. and Z.W.; supervision, K.W., H.X., and L.H.; funding acquisition, R.M. All authors have read and agreed to the published version of the manuscript.

**Funding:** This research was funded by National Natural Science Foundation of China (52071045 and 52271305), National Key R&D Program of China (2022YFB4300805), Fundamental Research Funds for Universities (LJKMZZ20220360 and LJKQZ2021009), High-tech Ship Research Project of China Ministry of Industry and Information Technology (2019360), and China Postdoctoral Science Foundation (2021T140080).

**Institutional Review Board Statement:** Not applicable.

**Informed Consent Statement:** Not applicable.

**Data Availability Statement:** All data are publicly available, and the sources of the data are provided in the paper.

**Conflicts of Interest:** The authors declare no conflict of interest.

## References

1. Parkes, A.I.; Sobey, A.J.; Hudson, D.A. Physics-based shaft power prediction for large merchant ships using neural networks. *Ocean Eng.* **2018**, *166*, 92–104.
2. Burel, F.; Taccani, R.; Zuliani, N. Improving sustainability of maritime transport through utilization of Liquefied Natural Gas (LNG) for propulsion. *Energy* **2013**, *57*, 412–420. [[CrossRef](#)]
3. Elgohary, M.M.; Seddiek, I.S.; Salem, A.M. Overview of alternative fuels with emphasis on the potential of liquefied natural gas as future marine fuel. *Proc. Inst. Mech. Eng. Part M J. Eng. Marit. Environ.* **2015**, *229*, 365–375.
4. Uyanık, T.; Karatug, Ç.; Arslanoğlu, Y. Machine learning approach to ship fuel consumption: A case of container vessel. *Transp. Res. Part D Transp. Environ.* **2020**, *84*, 102389.
5. Boden, T.A.; Andres, R.J.; Marland, G. *Global, Regional, and National Fossil-Fuel CO<sub>2</sub> Emissions (1751–2014)*; Carbon Dioxide Information Analysis Center: Oak Ridge, TN, USA, 2017.
6. Faber, J.; Hanayama, S.; Zhang, S.; Pereda, P.; Comer, B.; Hauerhof, E.; Loeff, W.S.; Smith, T.; Zhang, Y.; Kosaka, H.; et al. *Fourth IMO GHG Study 2020-Final Report Note by the Secretariat*; Marine Environment Protection Committee (MEPC): London, UK, 2020.
7. Lu, R.; Ringsberg, J.W. Ship energy performance study of three wind-assisted ship propulsion technologies including a parametric study of the Flettner rotor technology. *Ships Offshore Struct.* **2020**, *15*, 249–258.
8. Eyring, V.; Köhler, H.W.; Lauer, A.; Lemper, B. Emissions from international shipping: 2. Impact of future technologies on scenarios until 2050. *J. Geophys. Res. Atmos.* **2005**, *110*, D17.
9. Glykas, A.; Papaioannou, G.; Perissakis, S. Application and cost–benefit analysis of solar hybrid power installation on merchant marine vessels. *Ocean Eng.* **2010**, *37*, 592–602.
10. Bouman, E.A.; Lindstad, E.; Rialland, A.I.; Strømman, A.H. State-of-the-art technologies, measures, and potential for reducing GHG emissions from shipping—A review. *Transp. Res. Part D Transp. Environ.* **2017**, *52*, 408–421.
11. Xing, H.; Spence, S.; Chen, H. A comprehensive review on countermeasures for CO<sub>2</sub> emissions from ships. *Renew. Sustain. Energy Rev.* **2020**, *134*, 110222.
12. Nyanya, M.N.; Vu, H.B.; Schönborn, A.; Ölcer, A.I. Wind and solar assisted ship propulsion optimisation and its application to a bulk carrier. *Sustain. Energy Technol. Assess.* **2021**, *47*, 101397.
13. Mahmoodi, K.; Ghassemi, H.; Razminia, A. Wind energy potential assessment in the Persian Gulf: A spatial and temporal analysis. *Ocean Eng.* **2020**, *216*, 107674. [[CrossRef](#)]
14. Wang, K.; Xu, H.; Li, J.; Huang, L.; Ma, R.; Jiang, X.; Yuan, Y.; Mwero, N.A.; Sun, P.; Negenborn, R.R.; et al. A novel dynamical collaborative optimization method of ship energy consumption based on a spatial and temporal distribution analysis of voyage data. *Appl. Ocean Res.* **2021**, *112*, 102657. [[CrossRef](#)]
15. Yingjie, D.; Xianku, Z.; Guoqing, Z. Fuzzy logic based speed optimization and path following control for sail-assisted ships. *Ocean Eng.* **2019**, *171*, 300–310. [[CrossRef](#)]
16. Wang, K.; Xue, Y.; Xu, H.; Huang, L.; Ma, R.; Zhang, P.; Jiang, X.; Yuan, Y.; Negenborn, R.R.; Sun, P. Joint energy consumption optimization method for wing-diesel engine-powered hybrid ships towards a more energy-efficient shipping. *Energy* **2022**, *245*, 123155. [[CrossRef](#)]

17. Gkerekos, C.; Lazakis, I. A novel, data-driven heuristic framework for vessel weather routing. *Ocean Eng.* **2020**, *197*, 106887. [[CrossRef](#)]
18. Wang, K.; Li, J.; Yan, X.; Huang, L.; Jiang, X.; Yuan, Y.; Ma, R.; Negenborn, R.R. A novel bi-level distributed dynamic optimization method of ship fleets energy consumption. *Ocean Eng.* **2020**, *197*, 106802. [[CrossRef](#)]
19. Wang, K.; Li, J.; Huang, L.; Ma, R.; Jiang, X.; Yuan, Y.; Mwero, N.A.; Negenborn, R.R.; Sun, P.; Yan, X. A novel method for joint optimization of the sailing route and speed considering multiple environmental factors for more energy efficient shipping. *Ocean Eng.* **2020**, *216*, 107591. [[CrossRef](#)]
20. Wang, K.; Guo, X.; Zhao, J.; Ma, R.; Huang, L.; Tian, F.; Dong, S.; Zhang, P.; Liu, C.; Wang, Z. An integrated collaborative decision-making method for optimizing energy consumption of sail-assisted ships towards low-carbon shipping. *Ocean Eng.* **2022**, *266*, 112810.
21. Du, Y.; Meng, Q.; Wang, S.; Kuang, H. Two-phase optimal solutions for ship speed and trim optimization over a voyage using voyage report data. *Transp. Res. Part B Methodol.* **2019**, *122*, 88–114. [[CrossRef](#)]
22. Palomba, G.; Scattareggia Marchese, S.; Crupi, V.; Garbatov, Y. Cost, Energy Efficiency and Carbon Footprint Analysis of Hybrid Light-Weight Bulk Carrier. *J. Mar. Sci. Eng.* **2022**, *10*, 957. [[CrossRef](#)]
23. Hu, Y.; Li, R.; Du, L.; Ren, S.; Chevallier, J. Could SO<sub>2</sub> and CO<sub>2</sub> emissions trading schemes achieve co-benefits of emissions reduction? *Energy Policy* **2022**, *170*, 113252. [[CrossRef](#)]
24. Pauli, G. *Emissions and Inland Navigation. Green Transportation Logistics: The Quest for Win-Win Solutions*; Springer International Publishing: Cham, Switzerland, 2016; pp. 479–515.
25. Morvan, A.; Sacher, M.; Nême, A.; Leroux, J.B.; Jochum, C.; Abiven, N. Efficient jib-mainsail fluid-structure interaction modelling—Validations with semi-rigid sails experiments. *Ocean Eng.* **2022**, *243*, 110210. [[CrossRef](#)]
26. Du, W.; Li, Y.; Zhang, G.; Wang, C.; Zhu, B.; Qiao, J. Energy saving method for ship weather routing optimization. *Ocean Eng.* **2022**, *258*, 111771. [[CrossRef](#)]
27. Kramer, J.V.; Steen, S. Sail-induced resistance on a wind-powered cargo ship. *Ocean Eng.* **2022**, *261*, 111688. [[CrossRef](#)]
28. Lee, H.; Jo, Y.; Lee, D.J.; Choi, S. Surrogate model based design optimization of multiple wing sails considering flow interaction effect. *Ocean Eng.* **2016**, *121*, 422–436. [[CrossRef](#)]
29. Li, Q.; Nihei, Y.; Nakashima, T.; Ikeda, Y. A study on the performance of cascade hard sails and sail-equipped vessels. *Ocean Eng.* **2015**, *98*, 23–31. [[CrossRef](#)]
30. Elger, D.E.; Bentin, M.; Vahs, M. Comparison of different methods for predicting the drift angle and rudder resistance by wind propulsion systems on ships. *Ocean Eng.* **2020**, *217*, 108152. [[CrossRef](#)]
31. Sauder, T.; Alterskjær, S.A. Hydrodynamic testing of wind-assisted cargo ships using a cyber–physical method. *Ocean Eng.* **2022**, *243*, 110206. [[CrossRef](#)]
32. Ma, Y.; Bi, H.; Hu, M.; Zheng, Y.; Gan, L. Hard sail optimization and energy efficiency enhancement for sail-assisted vessel. *Ocean Eng.* **2019**, *173*, 687–699. [[CrossRef](#)]
33. Jia, X.L.; Yang, Y.S. *Mathematical Models for Ship's Modeling Control*; Dalian Maritime University: Dalian, China, 1999; pp. 49–138. (In Chinese)
34. Tillig, F.; Ringsberg, J.W. Design, operation and analysis of wind-assisted cargo ships. *Ocean Eng.* **2020**, *211*, 107603. [[CrossRef](#)]

**Disclaimer/Publisher's Note:** The statements, opinions and data contained in all publications are solely those of the individual author(s) and contributor(s) and not of MDPI and/or the editor(s). MDPI and/or the editor(s) disclaim responsibility for any injury to people or property resulting from any ideas, methods, instructions or products referred to in the content.